Real-time acousto-optic imaging using a high peak power long-pulsed illumination

François Fligliolia, Qin Liu, Sylvie Janicot, Patrick Georges, Gaëlle Lucas-Leclin, Jean-Pierre Huignard, Francois Ramaz, Jean-Michel Tualle, Maimouna Bocoum

To be published in Optics Letters:

Title: Real-time acousto-optic imaging using a high peak-power long-pulsed illumination

Authors: françois fligliolia,Qin Liu,Sylvie Janicot,Patrick Georges,Gaelle Lucas-Leclin,Jean-Pierre Huignard,Francois Ramaz,Jean-Michel Tualle,Maimouna Bocoum

Accepted: 21 September 24

Posted 23 September 24

DOI: https://doi.org/10.1364/OL.528953

Real-time acousto-optic imaging using a high peak power long-pulsed illumination

FRANÇOIS FIGLIOLIA[1], QIN LIU[2], SYLVIE JANICOT[2], PATRICK GEORGES[2], GAËLLE LUCAS-LECLIN[2], JEAN-PIERRE HUIGNARD[1], FRANÇOIS RAMAZ[1], JEAN-MICHEL TUALLE[3], AND MAÏMOUNA BOCOUM[1*]

[1] *ESPCI Paris, PSL University, CNRS, Institut Langevin, 75005 Paris, France*
[2] *Université Paris-Saclay, Institut d'Optique Graduate School, CNRS, Laboratoire Charles Fabry, 91127, Palaiseau, France*
[3] *Laboratoire de Physique des Lasers, CNRS, Université Sorbonne Paris Nord, 99 avenue J.-B. Clément, 93430 Villetaneuse, France*
[*] *maimouna.bocoum@espci.fr*

Compiled September 12, 2024

Acousto-optic imaging (AOI) of absorbing objects embedded in highly scattering media remains challenging since the detectable signal suitable for image reconstruction is weak. To increase the detected signals to a level required by live biological applications, we designed a high peak power quasi-continuous laser source based on the coherent combination of two pulsed amplifiers, delivering 100 µs-long pulses with a 9 W peak power at a 100 Hz repetition rate while maintaining an average power below 100 mW; jointly used with a digital holographic detection which maximises the amount of collected signal, we demonstrate for the first time the optical imaging of 2-cm-thick highly scattering media ($\mu_s' \sim 10$ cm^{-1}) at near video frame rate (0.2 Hz) using Fourier Transform-AOI.

http://dx.doi.org/10.1364/ao.XX.XXXXXX

1. INTRODUCTION

As light travels through biological tissues, photons undergo multiple scattering events, thus preventing in-depth direct imaging, which mainly relies on ballistic light [1]. Acousto-optic (AO) imaging [2] is therefore of seminal interest because it aims at imaging optical absorbers up to centimetre depths without prior knowledge of the medium scattering properties. In AO imaging (AOI), a spectrally narrow ($\sim$ MHz) laser illuminates the medium and ballistic ultrasonic waves (US) are used to tag the propagating photons. The signal obtained by filtering out these tagged photons is proportional to the local density of light, such that an image of the optical absorption can be obtained by sequentially varying the spatiotemporal profile of the US.

For *in-vivo* biomedical applications, the filtering process needs to be less than a millisecond to remain insensitive to the speckle decorrelation of biological tissues [3–5]. Moreover, aiming at generating close-to-video rate images requires relaxing any constraint on averaging by maximising the amount of tagged photons collected in a single acquisition. This implies resorting to optical detections with large optical *etendues*, such as spectral hole burning detection [6–8], lock-in cameras [9, 10] and digital holography [11, 12]. In addition, the tagged photons number can be further increased by properly choosing the insonification scheme. In that respect, images close to video rate (0.2 Hz) have recently been reported by relying on Fourier transform acousto-optic imaging (FT-AOI) [11, 12] which uses long periodic US pulses to tag photons. Photons were detected using off-axis holography with a camera integration time set to 100 µs, therefore compatible with the *in-vivo* requirement. Despite the clear advantage of FT-AOI over more traditional insonification schemes [12], single-shot acquisitions remained restricted to low scattering phantoms only ($\mu_s' \sim 1$ cm^{-1}, an order of magnitude less than biological tissues). To reach a sufficient signal-to-noise (SNR) ratio, our last resort is to increase the laser power while being mindful of the biomedical safety regulations [13] that cap the illumination intensity at 200 mW/cm^2 in the 400 nm – 1400 nm range. An increase in the laser peak power while maintaining a low average power is possible under quasi-continuous-wave (QCW) operation.

The use of QCW light to generate an AO signal was reported only once in the pioneering work of Monchalin et al. 20 years ago [14]. A 1064 nm CW laser seed was amplified with a flashlamp-pumped gain-switched amplifier, providing 500 W peak power pulses of 530 µs at a 25 Hz repetition rate. The first reported results [14] relied on a photorefractive detection scheme and a sample illumination of $\sim$ 100 W. However significant these high peak powers are, the authors do not mention any net gain in SNR provided by their source, and no further work based on QCW has since been reported. Indeed, flashlamps were replaced massively by narrower-linewidth diode pumps to improve stability and reduce the thermal load on the crystal known to generate detrimental lensing effects [15]. This latter point is crucial since a simultaneous increase in peak power and laser noise might not necessarily yield a net improvement in SNR, thereby not leading to any image quality enhancement. Finally, the use of the 1064 nm-wavelength in this work is out of the 650 nm $\leq \lambda \leq$ 900 nm therapeutic window where both haemoglobin and water optical absorption is low [16]. In this spectral range, semiconductor laser diodes configured as master-oscillator power amplifiers (MOPAs) are commonly used with CW optical power limited to the Watt level [17–19].

Here, we address the question of high-peak-power instabilities

by favouring semiconductor optical amplifiers operating at 828 nm. We developed a dedicated laser source based on the coherent combination of two amplifiers operating in parallel, seeded by a single narrow-linewidth laser diode. The laser source provides 100 µs-long pulses at a 100 Hz rate, with a maximum peak power of 8.2 W. Despite residual pulse-to-pulse power fluctuations at the 100 Hz acquisition rate of the camera, we obtained a substantial SNR improvement over the current state-of-the-art, leading to the first *in-vivo* compatible AO imaging inside thick and highly scattering media at near-video rates.

2. DESCRIPTION OF THE EXPERIMENTAL SETUP

The MOPA architecture presented here is similar to the one implemented in a previous experiment for lidar applications [20]. It is based on the coherent combination of two amplified beams seeded by the same laser source, using constructive interferences between them to sum their optical power. The master oscillator is a single-frequency fibre-coupled DBR laser diode (Photodigm, Inc., PH828DBR180T8), emitting a CW optical power of 100 mW at $\lambda = 828$ nm. The laser linewidth is estimated to be 0.5 MHz (from the datasheet), and the Side-Mode Suppression Ratio is better than 30 dB. To prevent possible parasitic optical feedbacks and maintain the laser spectral properties under operation, an optical isolator preceded by two Glan polarizers ensures excellent optical isolation (> 100 dB) of the DBR laser from the following elements. The laser beam is directed to a 50:50 PM single-mode fibre coupler to inject two tapered semiconductor optical amplifiers (TPA – Eagleyard Photonics, EYP-TPA-0830). Their gain spectrum is centred at 830 nm, and the amplified beams are linearly polarized. The injection power level is 26 mW to saturate the amplifiers and suppress amplified spontaneous emission [**Fig. 1**]. Each TPA is pulse-driven by a commercial

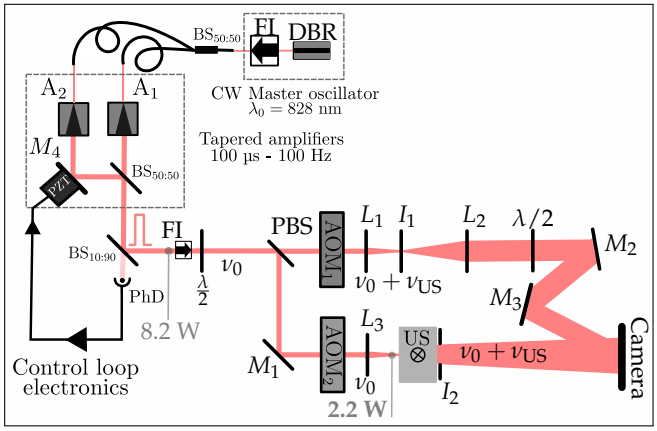

Fig. 1. Experimental set-up. $\lambda/2$: half-wave plate, PBS: Polarizing Beam Splitter. BS: Beam Splitter. AOM*i*: acousto-optic modulators. L_i : lenses, I_i: irises. M_i: mirrors. A_i: TPA. PZT: mirror attached on a piezoelectric transducer. PhD: photodiode.FI: Faraday isolator. US: ultrasonic probe. ν_0: laser carrier frequency. ν_{US}: ultrasounds frequency.

current driver (Arroyo Instruments 4320 Laser source) with a pulse duration of about 100 µs at a repetition rate of 100 Hz. The amplified pulse rise time, below 30 µs, is limited by the quasi-continuous wave (QCW) current driver performance. The amplifiers are operated at 7A, far above the CW driving current and before thermal rollover reduces the slope efficiency, achieving an output peak power of 5.5 W per TPA. The astigmatic amplified beams are collimated with a pair of aspheric ($f'_4 = 2.75$ mm) and cylindrical lenses ($f'_5 = 12.7$ mm), carefully positioned and glued onto the base plate to maintain stability [**Fig. 1**]. The amplified beams, combined in a Mach–Zehnder interferometer architecture, are carefully overlapped on a 50:50 beamsplitter in free space for constructive interferences [20, 21]. The dynamic nature of the QCW operation of the semiconductor amplifiers results in a rise of the device temperature during the 100 µs pulse, leading to the appearance of a thermal lens. This results in a measurable phase drift during the amplified pulse, and simultaneous dynamic change of the beam profile [**Fig. 2**][21]. At the maximal operation current of 7 A, the phase drift amplitude repeatably reaches 13π. Since the phase evolutions during the pulses are similar between the two amplified beams, with a maximal phase drift difference below 0.5π excluding the first 10 µs of the pulse, constructive interference between the two beams persists on the beamsplitter, and no phase correction is necessary during the pulse. However, differential phase fluctuations due to low-frequency thermal and acoustic noises arise for frequencies typically < 1 Hz and must be corrected to maintain a high combination efficiency. For that purpose, a portion of the combined power, measured on a photodiode followed by a sample-and-hold circuit feeds a gradient descent algorithm [20] that generates a path length correction voltage to the piezoelectric transducer attached to a folding mirror [**Fig. 1**]. The 5 Hz frequency bandwidth of this servo-loop is sufficient to maintain an efficient phase matching between the amplified pulses.

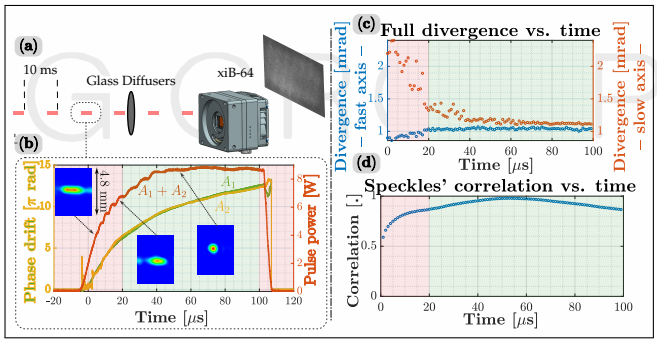

Fig. 2. (a) Scheme of acquisition. (b) Time profile of each TPA A_i and the coherently combined pulse $A_1 + A_2$. Images of recombined spatial modes at 10, 20 and 60 µs. (c) Evolution of the fast and slow axis spatial divergences during the pulse, measured 85 cm from the collimating lens. (d) Correlation of the instantaneous speckles and the averaged speckle.

As a result, we obtain a combined output peak power of 8 W, corresponding to a combining efficiency of 84% ± 4%, limited by residual mismatches in both spatial and temporal phase profiles. This combining efficiency is comparable with our previous results on TPA operating at different pulse regimes [20, 21].

Complex media are sensitive to the spatial mode of the illumination source. Thus, maintaining the SNR in an AO acquisition requires a stable profile of the amplified laser beam during the pulse to avoid self-induced speckle decorrelation [22]. Here, the evolution of the spatial mode during the pulse is recorded with a CMOS camera positioned 85 cm from the output of the collimating lens ([**Fig. 1**]: L_5). A 1 µs camera integration time enables sampling the beam profile at 100 different triggering times throughout the pulse; the beam divergence, estimated

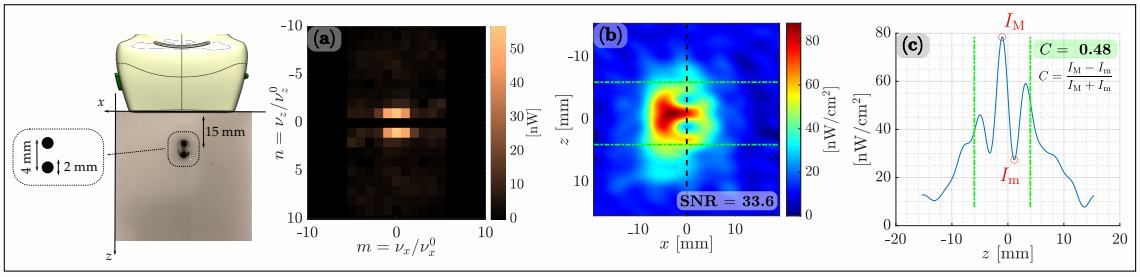

Fig. 3. FT-AOI image of two ink inclusions concealed within a 2-cm-thick scattering hydrogel ($\mu_s' = 5\,\mathrm{cm}^{-1}$) with a 2.2 W incident peak power on the gel. (a) Fourier component modulus with $(n, m) \in [-5; 5] \times [1; 10]$. (b) AO image obtained by inverse Fourier transform of (a). (c) Vertical intensity profile corresponding to the dotted black line of (b) with an estimation of the contrast in the region limited by the two green dotted lines. Left: phantom cross-section revealing the two ink inclusions – I_m and I_M are the maximum and minimum in the green dotted lines limited region.

with a Gaussian fit, evolves during the first 20 µs of the pulse before reaching stability, thereby providing a 80 µs-pulse window for AOI, indicated in green color[**Fig.** 2]. Speckle patterns were recorded in the transmission of a solid diffuser (Thorlabs N-BK7 Ground Glass Diffusers) with an integration time of 1 µs and at different times throughout the pulse[**Fig.** 2a]. The whole stack of frames reflects the speckle dynamic due to the in-pulse evolution of the spatial mode. We plot the correlation of the full-pulse averaged speckle with an instantaneous speckle over 100 different instants in [**Fig.** 2d]. As expected, the speckle correlation is high, except for the first 20 µs, justifying the restricted use of the pulse last 80 µs for AO imaging to benefit from our laser power increase fully.

We then perform the image in the transmission of a scattering Agar-Intralipid hydrogel (2% wt.) mimicking both optical and mechanical properties of soft biological tissues [23]; resorting to the FT-AOI, fully described in [11]. Frames are acquired in the Fourier domain by generating long spatiotemporally structured US waves. The holographic detection of the phase-modulated photons is performed using the local oscillator (LO) phase and amplitude-matched to the US tagging pulse. Two $5 \times 5 \times 2\,\mathrm{cm}^3$ phantoms are prepared with a scattering coefficient of respectively $\mu_s' = 5\,\mathrm{cm}^{-1}$ and $\mu_s' = 10\,\mathrm{cm}^{-1}$, the latter matching that of biological tissues [1]. In both phantoms, two 4-mm-long cylindrical ink inclusions with a 2 mm diameter, separated by 4 mm, are buried 5 mm from the surface, 15 mm below the US transducer array [**Fig.** 3]. The QCW laser source is split into a LO and a probe beam which illuminates the phantom [**Fig.** 1]. Accounting for the overall optical transmission from the laser output to our phantom [**Fig.** 1], the incident peak power is 2.2 W. The speckle pattern transmitted towards the camera carries a 10.9-µW-peak power collected on a 2.4-cm^2-surface sensitive camera (Ximea xiB-64) of 4704×3424 pixels: that is a 7-fold increase in power compared to the CW laser source (MOPA, Sacher Lasertchnik) used in our previous experiments [12].

Photons are tagged with a 192-element linear transducer array (AixPlorer SL10-2) with a carrier frequency set to 3 MHz. The Fourier components $(m\nu_x^0, n\nu_z^0)$, where $(m, n) \in [-5; 5] \times [1; 10]$ are the harmonic orders used for the acquisition and ν_x^0 and ν_z^0 the fundamental frequencies in respectively x and z direction. The corresponding transverse spatial resolutions of the image are $\max(m)/(2\nu_x^0) = 3.3$ mm and $\max(n)/(2\nu_z^0) = 1.6$ mm: enough to discriminate the two inclusions with a $30 \times 30\,\mathrm{mm}^2$ field of view. For each frequency component (n, m), the complex Fourier coefficient is obtained by combining 4 frames where only the LO's phase is varied [11]. As a result, single-shot imaging requires the acquisition of $4 \times 110 = 440$ frames. Each frame is processed on a GPU (NVIDIA GTX 1080Ti) running customed highly parallelized computations such that the post-treatment is negligible compared to the acquisition time. At a 100 Hz repetition rate, this enables us to generate an AO image every 4.4 s, corresponding to a near-video rate of ~ 0.2 Hz. This imaging rate could be enhanced either by decreasing the targeted resolution of the imaging system – which would lower the required frame number and therefore the overall acquisition time, by increasing the laser repetition rate up to the camera's maximum frame rate of 300 Hz – which would require to reduce the pulse duration to maintain the laser duty cycle to its current value which is the maximum one the TPA can work with, or by doing sparse imaging – *i.e.* making hypothesis on the object we want to image to measure fewer Fourier components.

3. RESULTS

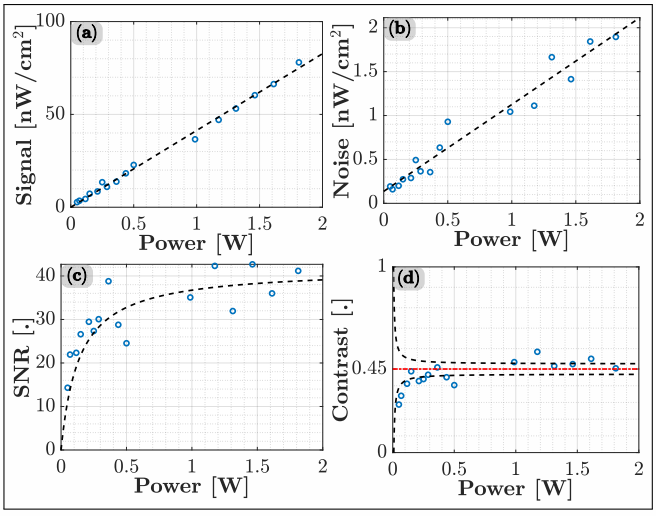

Fig. 4. (a) Signal and (b) noise obtained experimentally (circles) and their respective linear fits (black dotted line) as a function of incident peak power, for $\mu_s' = 5\,\mathrm{cm}^{-1}$. (c) SNR, calculated from (a) and (b). (d) AO images contrast and the 1-σ confidence interval (black dotted-line) deduced from (c). Red line: contrast convergence value.

AO images are first performed through the $\mu_s' = 5\,\mathrm{cm}^{-1}$ 2-cm-thick gel. The acquired Fourier components $\tilde{I}(m\nu_x^0, n\nu_z^0)$ filling

the Fourier plane are shown in [**Fig.** 3a]. The inverse Fourier transform of $\tilde{I}(mv_x^0, nv_z^0)$ provides the AO image [**Fig.** 3b], revealing the two absorbing inclusions. The longitudinal profile along the two inclusions is plotted in [**Fig.** 3c], from which we estimated the absorption contrast of $C = 0.48$. The same acquisition is reproduced by varying the incident peak power from 50 mW to 2.2 W while maintaining the LO peak power constant to 358 µW. The signal is defined as the maximum pixel value of the AO image and the noise as the standard deviation of the pixel values outside the laser halo in the AO image; the resulting SNR and the contrast are extracted and respectively plotted in [**Fig.** 4a-b-c-d]. As expected, the signal increases linearly with the probe peak power [**Fig.** 4a]. At zero power, the noise level reaches an offset set by the LO intrinsic noise and then follows a linear increase (as plotted in [**Fig.** 4b]) which is a characteristic feature of residual classical noise, which justifies the affine model [**Fig.** 4b] and is to be expected from any residual thermal lensing. These linear and affine models help to predict an SNR trend [**Fig.** 4c], where it increases with power before reaching an asymptotic value of 41.8. Preventing this saturation effect would require a further reduction of any classical noise, which means pushing the stability of the laser to its classical limit during one camera integration time, *i.e.* for frequency typically greater than 10 kHz. The contrast vs. the incident power is plotted [**Fig.** 4d] with a σ-confidence interval estimated from the uncertainty propagation of the SNR model previously obtained; for a contrast value of 0.45, the σ-confidence interval well contains the experimental data.

Finally, images performed in the $\mu_s' = 10\,\mathrm{cm}^{-1}$ phantom (2-cm-thick) [**Fig.** 5] mimicking a biological sample. From the raw image [**Fig.** 5a], additional corrections are undertaken to improve the image reconstruction quality and the SNR. First, Fourier components are normalized by the average value of each acquired hologram [**Fig.** 5b], thus limiting the low-frequency fluctuations effects on the reconstructed image. Then, to overcome the experimental difficulty of measuring the Fourier harmonics $n = 0$, the average value of each AO image's column is subtracted from the final AO image [**Fig.** 5c]. The resulting SNR of 19.2 ± 2.3 is approximately 12 times higher than previously reported images for a similar phantom but twice thinner than the sample herein used [12]. The imaging technique thus greatly benefits from the significant optical power increase during the camera integration time, meaning that the laser source properties are stable enough to prevent the speckle decorrelation.

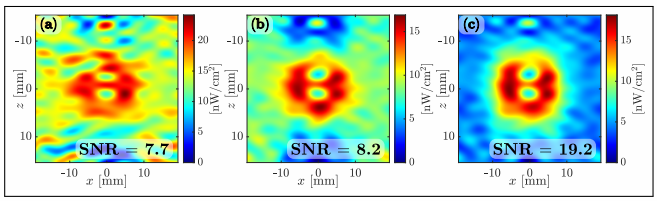

Fig. 5. Single-shot FT-AOI image for the $10\,\mathrm{cm}^{-1}$ phantom. (a) Raw image. (b) Image obtained by normalizing the Fourier components by the hologram average power. (c) Image obtained from (b) by adding an average value to compensate the unmeasured Fourier harmonics for $n = 0$.

4. CONCLUSIONS

We demonstrated how combining a tailored powerful QCW laser source based on an advanced laser architecture with the FT-AOI imaging technique enables to probe efficiently phantoms with a scattering coefficient matching that of biological tissues, with no need for signal averaging. Two noise sources remained as a limit to the highest reachable SNR. Firstly, high-frequency classical noise, typically over 10 kHz, mostly due to thermal lensing during the amplification, may lead to a self-induced decorrelation of the transmitted speckle; to limit this effect, we selected a part of the pulse where this effect was minimized. Secondly, low-frequency intensity noise at the camera frame rate induces frame-to-frame fluctuations of the signal; this is less detrimental since it can be measured, for instance on the zero order of the hologram, and included in the image reconstruction. Addressing both of these limitations, we performed single-shot acquisition schemes on a phantom mimicking the scattering strength of biological tissues ($\mu_s' = 10\,\mathrm{cm}^{-1}$) at 0.2 Hz. We are currently working on a further reduction of the laser classical noise and an increased number of coherently combined amplifiers to reach even higher SNR, thereby paving the way towards state-of-the-art deep acousto-optic imaging of highly scattering media.

Funding. Agence Nationale de la Recherche (ANR-21-CE42-0014).

Acknowledgments. This project has received financial support from the CNRS through the MITI interdisciplinary programs.

Disclosures. The authors declare no conflicts of interest.

Data Availability Statement. Data underlying the results presented in this paper may be obtained from the authors upon reasonable request.

REFERENCES

1. V. Ntziachristos, Nat. methods **7**, 603 (2010).
2. W. Leutz and G. Maret, Phys. B: Condens. Matter **204**, 14 (1995).
3. M. M. Qureshi, J. Brake, H.-J. Jeon, *et al.*, Biomed. Opt. Express **8**, 4855 (2017).
4. Y. Liu, P. Lai, C. Ma, *et al.*, Nat. Commun. **6**, 5904 (2015).
5. X. Wang, W. Zhao, A. Zhai, and D. Wang, Opt. Express **31**, 32287 (2023).
6. J. Gunther, A. Walther, L. Rippe, *et al.*, J. Biomed. Opt. **23**, 071209 (2018).
7. C. Venet, M. Bocoum, J.-B. Laudereau, *et al.*, Opt. Lett. **43**, 3993 (2018).
8. Q. M. Thai, G. Kalot, C. Venet, *et al.*, Biomed. optics express **13**, 6484 (2022).
9. Y. Liu, C. Ma, Y. Shen, and L. V. Wang, Opt. letters **41**, 1321 (2016).
10. K. Barjean, K. Contreras, J.-B. Laudereau, *et al.*, Opt. letters **40**, 705 (2015).
11. M. Bocoum, F. Figliolia, J.-P. Huignard, *et al.*, Appl. Opt. **62**, 4740 (2023).
12. L. Dutheil, M. Bocoum, M. Fink, *et al.*, Appl. optics **60**, 7107 (2021).
13. "Norm NF EN 60825, afnor edition (2008)," .
14. G. Rousseau, A. Blouin, and J.-P. Monchalin, Opt. Express **16**, 12577 (2008).
15. R. L. Byer, Science **239**, 742 (1988).
16. K. Singh, *Small Molecule Probes for Photodynamic Therapy (PDT)* (University of Toronto (Canada), 2019).
17. M. Chi, O. B. Jensen, J. Holm, *et al.*, Opt. express **13**, 10589 (2005).
18. B. Sumpf, K.-H. Hasler, P. Adamiec, *et al.*, IEEE J. Sel. Top. Quantum Electron. **15**, 1009 (2009).
19. G. Blume, J. Pohl, D. Feise, *et al.*, Opt. Lett. **40**, 1757 (2015).
20. Q. Liu, S. Janicot, P. Georges, and G. Lucas-Leclin, Opt. Lett. **48**, 489 (2023).
21. P. Albrodt, M. Niemeyer, P. Crump, *et al.*, Opt. Express **27**, 27891 (2019).
22. K. Kim, H. Yu, K. Lee, and Y. Park, Sci. Reports **7**, 44435 (2017).
23. S. L. Jacques, Phys. Med. Biol. **58**, R37 (2013).

FULL REFERENCES

1. V. Ntziachristos, "Going deeper than microscopy: the optical imaging frontier in biology," Nat. methods **7**, 603–614 (2010).
2. W. Leutz and G. Maret, "Ultrasonic modulation of multiply scattered light," Phys. B: Condens. Matter **204**, 14–19 (1995).
3. M. M. Qureshi, J. Brake, H.-J. Jeon, *et al.*, "In vivo study of optical speckle decorrelation time across depths in the mouse brain," Biomed. Opt. Express **8**, 4855–4864 (2017).
4. Y. Liu, P. Lai, C. Ma, *et al.*, "Optical focusing deep inside dynamic scattering media with near-infrared time-reversed ultrasonically encoded (TRUE) light," Nat. Commun. **6**, 5904 (2015).
5. X. Wang, W. Zhao, A. Zhai, and D. Wang, "Efficiently scanning a focus behind scattering media beyond memory effect by wavefront tilting and re-optimization," Opt. Express **31**, 32287–32297 (2023).
6. J. Gunther, A. Walther, L. Rippe, *et al.*, "Deep tissue imaging with acousto-optical tomography and spectral hole burning with slow light effect: a theoretical study," J. Biomed. Opt. **23**, 071209–071209 (2018).
7. C. Venet, M. Bocoum, J.-B. Laudereau, *et al.*, "Ultrasound-modulated optical tomography in scattering media: flux filtering based on persistent spectral hole burning in the optical diagnosis window," Opt. Lett. **43**, 3993–3996 (2018).
8. Q. M. Thai, G. Kalot, C. Venet, *et al.*, "In vivo ultrasound modulated optical tomography with a persistent spectral hole burning filter," Biomed. optics express **13**, 6484–6496 (2022).
9. Y. Liu, C. Ma, Y. Shen, and L. V. Wang, "Bit-efficient, sub-millisecond wavefront measurement using a lock-in camera for time-reversal based optical focusing inside scattering media," Opt. letters **41**, 1321–1324 (2016).
10. K. Barjean, K. Contreras, J.-B. Laudereau, *et al.*, "Fourier transform acousto-optic imaging with a custom-designed cmos smart-pixels array," Opt. letters **40**, 705–708 (2015).
11. M. Bocoum, F. Figliolia, J.-P. Huignard, *et al.*, "Suppression of the Talbot effect in Fourier transform acousto-optic imaging," Appl. Opt. **62**, 4740–4746 (2023).
12. L. Dutheil, M. Bocoum, M. Fink, *et al.*, "Fourier transform acousto-optic imaging with off-axis holographic detection," Appl. optics **60**, 7107 (2021).
13. "Norm NF EN 60825, afnor edition (2008)," .
14. G. Rousseau, A. Blouin, and J.-P. Monchalin, "Ultrasound-modulated optical imaging using a powerful long pulse laser," Opt. Express **16**, 12577–12590 (2008).
15. R. L. Byer, "Diode laser—pumped solid-state lasers," Science **239**, 742–747 (1988).
16. K. Singh, *Small Molecule Probes for Photodynamic Therapy (PDT)* (University of Toronto (Canada), 2019).
17. M. Chi, O. B. Jensen, J. Holm, *et al.*, "Tunable high-power narrow-linewidth semiconductor laser based on an external-cavity tapered amplifier," Opt. express **13**, 10589–10596 (2005).
18. B. Sumpf, K.-H. Hasler, P. Adamiec, *et al.*, "High-Brightness Quantum Well Tapered Lasers," IEEE J. Sel. Top. Quantum Electron. **15**, 1009–1020 (2009).
19. G. Blume, J. Pohl, D. Feise, *et al.*, "Single-mode master-oscillator power amplifier at 647 nm with more than 500 mw output power," Opt. Lett. **40**, 1757 (2015).
20. Q. Liu, S. Janicot, P. Georges, and G. Lucas-Leclin, "Coherent combination of micropulse tapered amplifiers at 828 nm for direct-detection LIDAR applications," Opt. Lett. **48**, 489–492 (2023).
21. P. Albrodt, M. Niemeyer, P. Crump, *et al.*, "Coherent beam combining of high power quasi continuous wave tapered amplifiers," Opt. Express **27**, 27891–27901 (2019).
22. K. Kim, H. Yu, K. Lee, and Y. Park, "Universal sensitivity of speckle intensity correlations to wavefront change in light diffusers," Sci. Reports **7**, 44435 (2017).
23. S. L. Jacques, "Optical properties of biological tissues: a review," Phys. Med. Biol. **58**, R37–61 (2013).